J Nanopart Res (2012) 14:803
DOI 10.1007/s11051-012-0803-y

RESEARCH PAPER

New gasochromic system: nanoparticles in liquid

M. Ranjbar · H. Kalhori · S. M. Mahdavi · A. Iraji zad

Received: 26 October 2011 / Accepted: 26 February 2012

Abstract In this study, WO_3 nanocrystallites were first produced by laser ablation of W target in deionised water. To synthesize palladium, a $PdCl_2$ solution (0.2 g/L) was added to the liquid. Transmission electron microscope revealed successful synthesis of tungsten oxide nanocrystallites along with the production of Pd and core–shell Pd/WO_3 nanoparticles. Gasochromic behavior was examined by hydrogen bubbling into Pd/WO_3 liquid in which a transition to blue absorbing state was observed. Optical absorption spectra of the colored liquid represented different sharp small polaron absorbing peaks below 3 eV and the peaks intensity was observed to be varied with $Pd:WO_3$ ratio. Time variations of optical density difference (ΔOD) were measured at constant wavelength of 632.8 nm by alternative bubbling hydrogen or oxygen gases. The ΔOD in the first coloring cycles were not completely reversible owing to the presence of some unreacted $PdCl_2$. The further coloring bleaching indicates a normal gasochromic behavior.

Keywords Gasochromic · Pulsed laser ablation (PLA) · WO_3 nanocrystallite · $PdCl_2$ · Pd nanoparticles

M. Ranjbar (✉)
Department of Physics, Isfahan University of Technology, Isfahan 84156-83111, Iran
e-mail: ranjbar@cc.iut.ac.ir

H. Kalhori · S. M. Mahdavi (✉) · A. Iraji zad
Physics Department, Sharif University of Technology, P.O. Box 11155, 9161 Tehran, Iran
e-mail: mahdavi@sharif.edu

S. M. Mahdavi · A. Iraji zad
The Institute for Nanoscience and Nanotechnology (INST), Sharif University of Technology, P.O. Box 11155, 9161 Tehran, Iran

Introduction

Today tungsten oxide layers and coatings have become more applicable in science and technology because of their catalytic and sensing properties against many types of gases (Li et al. 2004; Cantalini et al. 1996) and also for their electrochromic and gasochromic properties for solar applications (Granqvist 1995; Zayat et al. 1998; Georg et al. 2000; Lee et al. 2001). In the gasochromic phenomenon, tungsten oxide films activated with a thin Pd or Pt layer are optically switchable from a bleach or transparent state to a dark blue absorbing state when they are exposed to H_2 gas. This process is reversible; when H_2 is replaced with O_2, the colored state reversibly turns to the bleach state. The light absorption is attributed to the formation of small polarons as quasi particle states as a result of the H_2 intercalation of with WO_3 lattice (Lee et al. 2001; Niklasson and Granqvist 2007). Up to now many groups have been studied the gasochromic tungsten oxide films, containing Pd or Pt catalyst, on different substrates by conventional deposition techniques such as sputtering(Abrutis et al. 2004), sol–gel

Published online: 14 March 2012

(Zayat et al. 1998), evaporation(Antonaia et al. 1999), and Pulsed laser deposition (PLD) (Ranjbar et al. 2010; Ranjbar et al. 2008a; Ranjbar et al. 2008b).

Recently liquid nanoparticle media are proposed as a means to enhance solar absorption efficiency through direct absorption of the incoming solar energy (Prasher et al. 2005). Accordingly, similar to planar gasochromic systems (coatings and films), an optically switchable liquid brings more advantages for solar applications because in this approach, the tuning and optimization of absorbing light is possible. To explore a switchable gasochromic liquid system, in which optical properties can change by hydrogen incorporation, a colloidal dispersion of WO_3 nanoparticles activated with palladium may be a predominantly candidate.

In this study, nanocrystallites of WO_3 were fabricated by laser ablation of W target in water environment. Then it was attempted to attach palladium nanoparticles to the surface of tungsten oxide nanocrystallites through a seed-mediated growth process. In the fabrication of nanoparticle by laser ablation, the beam of a pulsed laser is focused on a target placed in the liquid. The initial process of laser ablation is the interaction of light with the solid target surface, which causes vaporization of the solid target and a small amount of surrounding liquid. Chemical reactions between the ablated species and molecules in the liquid can subsequently occur, as the ejected species are highly excited, both electronically and translationally (Sakka et al. 2000) The reaction products are typically nanoparticles composed of atoms from both the target and the liquid, which form a suspension in the liquid. Moreover, the energetic metal species can react and are quenched when they enter in contact with water molecules, forming nuclei of oxide or hydroxide via instantaneous hydrothermal oxidation (Sasaki et al. 2006). Hence, it is expected that the laser ablation of a W target in water results in nucleation and growth of tungsten oxide nanoparticles.

Attachment of palladium to WO_3 nanocrystallites and formation core–shell structures should be crucial for activation the liquid against the hydrogen gas. The preparation methods of core–shell nanoparticles reported so far is divided into two categories: successive and simultaneous. The simultaneous methods proceed with the precursors of the two metals present in a same reaction system. The successive methods involve reducing shell ions on the surface of the preformed core seeds (Hu et al. 2007). In this study, Pd shells were produced by adding a reactive solution involving Pd^{2+} ions, such as $PdCl_2$ solution, into the WO_3 nanoparticle liquid (the successive method). Pd nanoparticles can be produced by an autocatalytic reaction, which occurs at the liquid–solid interface between a WO_3 NP surface and surrounding liquid. This process involves electron transfer across the surface following by a reduction–oxidation process. Previously we have used $PdCl_2$ solution for nucleation of Pd nanoparticles over the surface of WO_3 films. Pd^{2+} ions are reduced auto-catalytically or through hydrogen reduction (Ranjbar et al. 2010, 2011). It is expected that $PdCl_2$ solution act as a precursor of Pd for assembly of Pd/WO_3 nanoparticles.

Experimental

Tungsten oxide nanocrystallites were fabricated by laser ablation of tungsten target (99.9 % purity) in DI water. The ablation was carried out by first harmonic ($\lambda = 1064$ nm) beam of a Nd:YAG laser focused normal to the surface of target placed in water. The laser energy was 320 mJ and the repetition rate was 10 Hz for total 10 min. A $PdCl_2$ solution were prepared by adding 0.02 g $PdCl_2$ powder (99.99 % purity) into 99.9 cc DI water, and 0.1 HCl. This wet composition was kept in the ultrasonic bath for 3 h, and finally a uniform yellowish solution was achieved. To prepare different Pd/WO_3 ratio, varying amounts of $PdCl_2$ solution including 0.5, 1, 2, 3, and 4 cc, were added to 6 cc of as prepared liquid. These samples were named as $S_{0.5}$, S_1, S_2, S_3, and S_4. Then the mixed $PdCl_2$–WO_3 solutions were allowed to be stabilized for approximately 30 min. For surface chemistry analysis, a sample was prepared by drop-drying of WO_3 liquid over a silicon substrate. Surface analysis of the samples was done in an ESCA/AES system. The system is equipped with a concentric hemispherical analyzer (CHA, Specs model EA10 plus) suitable for Auger electron spectroscopy and X-ray photoelectron spectroscopy (XPS). For exciting the X-ray photoelectrons, an Al Kα line at 1486.6 eV was used. The energy scale was calibrated against the carbon binding energy (284.8 eV). Optical properties of liquids before and after hydrogen intercalation were measured in the 200–1200 nm wavelength range using a Lambda 950 spectrophotometer (Perkin Elmer). Size and morphology of the produced nanoparticles were observed on

Philips 200 transmission electron microscope (TEM). The gasochromic experiments were carried out by alternatively bubbling 10 %H_2/Ar (flow = 60 l/h) or O_2 (flow = 30 l/h) gases through a tiny stainless steel pipe into a quartz cell containing WO_3–$PdCl_2$ solution. A beam of He–Ne laser ($\lambda = 632.8$ nm) was delivered from one side to the center of liquid in the quartz cell and a detector on the other side used for recording the time variations of optical transmission. The tiny pine was mounted in the corner of the cell in such a way that the bubbles were not crossing the laser beam and no light scattering by bubbles was observed. The details are shown in Fig. 1. The dynamic response was measured during the bubbling by converting the detector current into the light intensity according to its datasheet guide. To avoid hydrogen removal from the liquid after the full coloring of each sample, the cell became immediately sealed in the steam of bubbling hydrogen, and then it was transferred into the spectrophotometer. The bleach spectra were recorded 30 min. after opening the sealed cell in oxygen atmosphere.

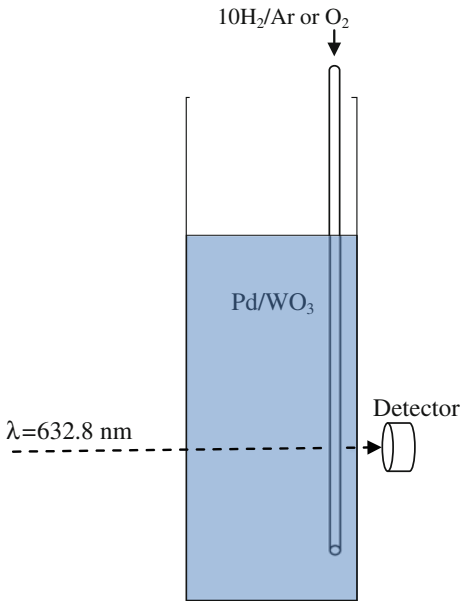

Fig. 1 Schematic of gasochromic test setup for Pd/WO_3 in water as gasochromic liquid

Result and discussion

Synthesis of tungsten oxide nanocrystallites and Pd nanostructures

Laser ablation of W target in water did not lead to transform the transparency of liquid considerably. To determine the chemical state of species in liquid medium, we applied XPS technique on a drop-dried WO_3 coating on a clean silicon substrate. The high-resolution W_{4f} XPS spectrum is shown in Fig. 2a. The spectrum is decomposed into different doublet peaks. The doublet on binding energies of 35.7 and 37.8 eV is attributed to $W_{4f5/2}$ and $W_{4f7/2}$, respectively, and is at the same binding energy of tungsten atoms with +6 formal oxidation number as in WO_3 (Martin-Litas et al. 2002). A general agreement exists for the binding energies of W^{6+} at 35.7 and 37.7 eV (Di Gregorio and Keller 2004; Occhiuzzi et al. 2004). Furthermore, two additional peaks are located around 34.7 and 36.8 eV. According to literature, this doublet is originated from W^{5+} (Colton et al. 1978). The chemical state of oxygen is determined by high-resolution XPS spectra of O_{1s}, shown in Fig. 2b. This peak was deconvoluted

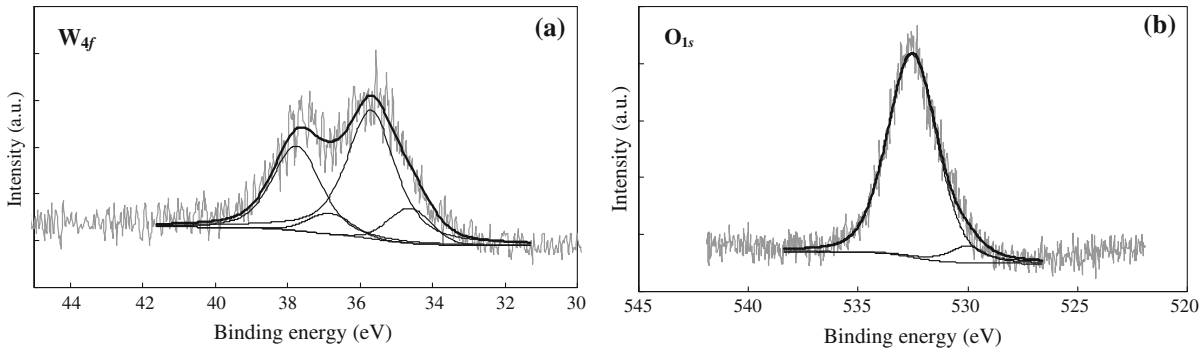

Fig. 2 High resolution XPS spectra of **a** W_{4f} and **b** O_{1s} corresponding to ablation of W target in DI water

into two peaks, one with low intensity at 530 eV and other with high intensity at 532.5 eV. According to literature, the first originates from oxygen in binding with tungsten atoms and the latter is due to surface oxygen absorbed from air or O–H groups. Since the WO_3 nanoparticles were produced in water environment, presence of O–H bonds is expected. Considering $W_{4f3/2}$ and O_{1s} (530 eV), the ratio of O/W was determined as ~ 3. In general, tungsten does not react with oxygen at room temperature but at elevated temperatures, WO_3 is forming. However, one can observe that the high power pulses of laser can assist the reaction of tungsten and oxygen at the liquid–solid interface even when the liquid kept at room temperature. In general, four kinds of chemical reactions would take place in the laser-induced plasma and the interface between the liquid and the laser-induced plasma during the transformation of the laser-induced plasma, respectively. In one of these regimes, the chemical reactions between the species from the laser ablating target and the species from the liquid molecules' excitation would occur inside the laser-induced plasma (Yang 2007). Therefore, in the laser ablation of tungsten target in water, W atoms can react with O atoms to form tungsten oxide nanocrystallites.

To create catalytic activity against hydrogen inside the liquid, different volumes of aqueous solution of 0.1 g/L $PdCl_2$ were added to the WO_3 nanocrystallite liquid. We observed an interesting effect when the as prepared WO_3 liquid (used immediately after laser ablation terminated) utilized. We visually observed a rapid change in the yellowish color of the filling $PdCl_2$ drops toward grayish color. This color transformation was not observed for liquid samples that were allowed to age at ambient condition for more than ~ 30 min. Depending on its concentration, a suspension of Pd particles has a grayish to darkish view so this observation suggests an enhanced autocatalytic reduction of $PdCl_2$ droplets as filling into the as-prepared liquid. Therefore, we attribute this effect to a fast process by which Pd^{2+} ions reduce to metal Pd nucleus due to the charge transfer between ions and WO_3 nanoparticles surface according to chemical reaction:

$$Pd^{2+} + 2e^- \rightarrow Pd^0 \quad (1)$$

Here, one can assume that the nucleation and growth of tungsten or tungsten oxide clusters do not terminate immediately, but instead it continues due to the small size and accessible unfilled bonds at their active surface. The consequence activity loss originates from the gradual surface passivation of nanoparticles for example through the increase in the particle size (decrease in surface/volume ratio), surface oxidation, and/or particle agglomeration.

In order to investigate the morphological properties and the shape of the WO_3 and Pd/WO_3 nanoparticles, we utilized Transmission electron microscopy (TEM). TEM images of WO_3 nanocrystallites before and after palladium adding are shown in Fig. 3a, b, respectively. From part (a) and corresponding size distribution histogram, various WO_3 nanocrystals with average size of ~ 40 nm are observable. Crystalline shape of the particles is obvious from the grain boundaries, which is in consistence with the electron diffraction pattern in the inset. Part (b), relevant to Pd/WO_3 sample, involves small particles and some larger core–shell particles. As illustrated by arrows, a porous Pd layer with approximately 10-nm thickness was formed on the perfect WO_3 nanocrystals. The porosity of Pd shell provides efficient hydrogen diffusion into the tungsten oxide lattice. The WO_3 nanocrsytals act as seeds for nucleation of Pd shells similar to what happens in seed-mediated growth process (Berhault et al. 2007). Furthermore, many distributed small particles are observed among the core–shell particles that are attributed to those individual metallic Pd nanoparticles that were produced spontaneously.

Optical properties of gasochromically colored liquid

The gasochromic switching behavior of Pd/WO_3 liquid was examined by the bubbling of hydrogen or oxygen gases into the liquid containing cell. Figure 4 shows a photograph image of sample S_1 before and after hydrogen bubbling illustrating the possibility of the gasochromic coloring of the Pd/WO_3 liquid. Except for the first coloring cycle, this effect is completely reversible and when the colored sample is exposed to air, its blue color coverts to the gray state. The first coloring cycle involves the hydrogen reduction of unreacted $PdCl_2$ and consequently a slight residual coloration is formed. The bleaching process also becomes faster if the hydrogen gas is replaced with pure oxygen gas. In this study, we used pure oxygen gas in all bleaching processes.

The optical properties of these types of Pd/WO_3 liquids were evaluated using UV–Visible transmission

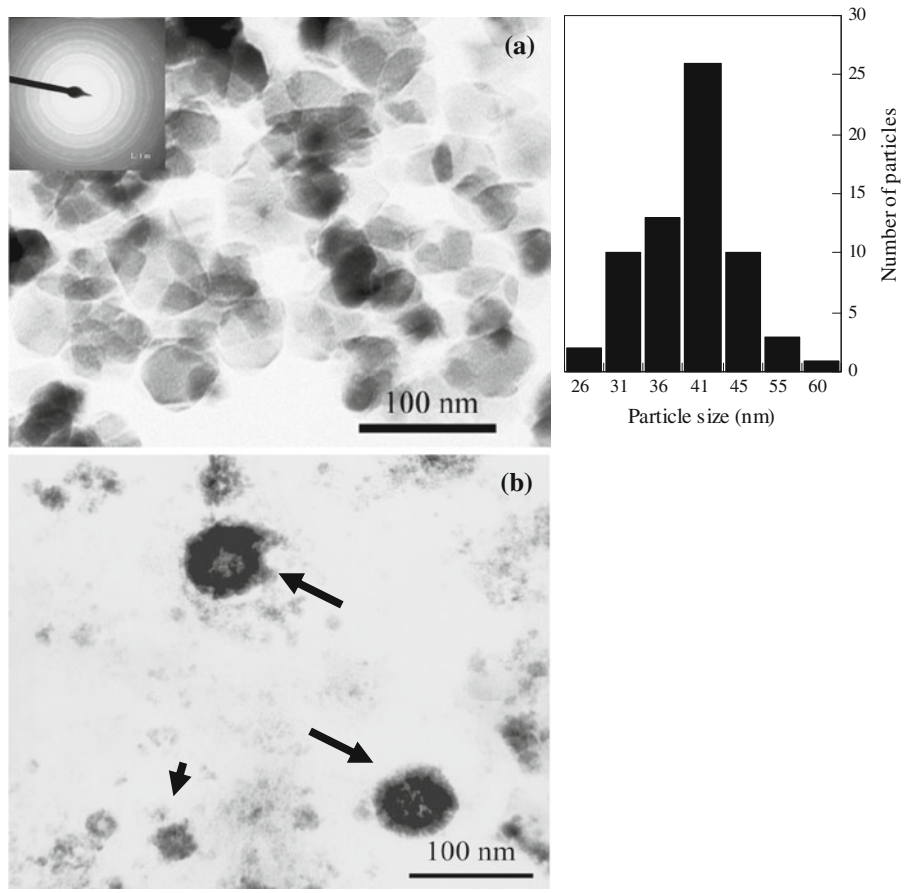

Fig. 3 TEM images of WO_3 nanocrystallites prepared by laser ablation of W in DI water and **a** before and **b** after adding $PdCl_2$. The size distribution *histogram of images* (**a**) is also shown

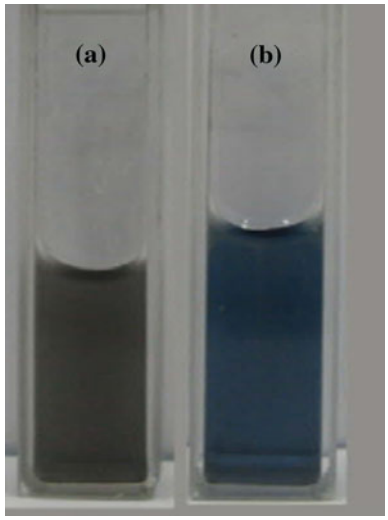

Fig. 4 Photograph images of Pd/WO_3 nanoparticle liquid **a** before and **b** after hydrogen incorporation. The *grayish color* of the sample (**a**) is due to reduced Pd metal nanoparticles and the blue color in part (**b**) is due to gasochromically coloring of WO_3 nanoparticles

in normal incident. Transmittance spectra in the range of 320–1,200 nm for a concentration range of $PdCl_2$ before and after hydrogen bubbling are shown in Fig. 5. Typical transmission spectrum of hydrogen-free (virgin) WO_3 liquid sample, shown at the top of Fig. 5, presents a highly visible transparency, and the relevant optical band gap energy was calculated about 3.5 eV which is in accordance with those reported for WO_3 (Ranjbar et al. 2008a). Although the optical transmittance reduces by increasing $PdCl_2$ concentration due to low transparency of palladium, the shoulders of optical band gap of the curve are clear for almost all the samples. The bottom of Fig. 5 shows that the near IR transmission of all the samples decreases by hydrogen incorporation. Moreover, depending upon the $PdCl_2$ contents, a number of certain absorption peaks appear in the spectra backgrounds. To give a better description, the absorption coefficient, α, of each sample versus photon energy before and after hydrogen intercalation are shown in

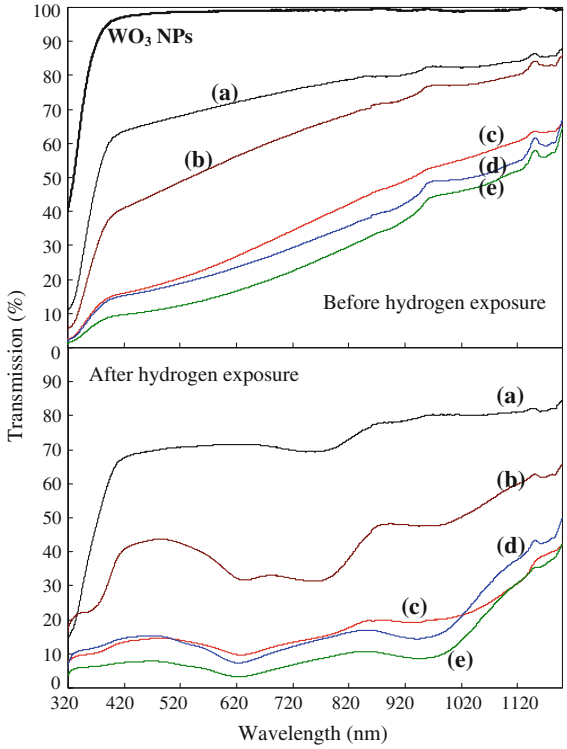

Fig. 5 Optical transmission spectra before and after hydrogen exposure for different samples of: **a** $S_{0.5}$, **b** S_1, **c** S_2, **d** S_3, and **e** S_4

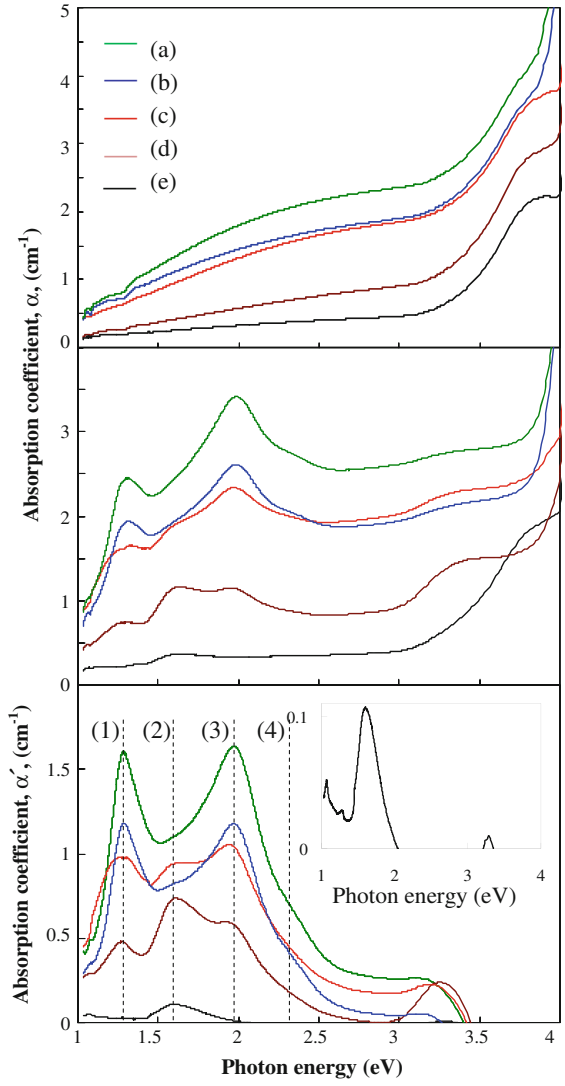

Fig. 6 Absorption coefficients of Pd/WO_3 nanoparticles in water before and after hydrogen exposure for different samples of: **a** $S_{0.5}$, **b** S_1, **c** S_2, **d** S_3, and **e** S_4

Fig. 6a, b). The rising magnitude of absorption coefficient above 3 eV is due to absorption across the optical band gap. To analyze the contribution of optical band gap, we also subtracted the absorption coefficient for hydrogen-free samples from that of the intercalated ones. The results are shown in Fig. 6c which is denoted α'. The effects of hydrogen bubbling into the liquid, creates several sharp absorption peaks at different photon energy. They are identified by the numbers (1), (2), (3), and (4), corresponding to the energies $\sim$1.32, 1.67, 1.96, and 2.38 eV, respectively. Similar to the light absorption in bronze tungsten oxide films resulting from the proton (gasochromic) or alkali ion intercalation (electrochromic) into the material, the IR absorption peaks of WO_3 nanoparticle liquid are attributed to a hydrogen intercalation effect. The changes in the optical density during the coloration are best described theoretically by the small polaron concept, or by the intervalence charge transfer model. Local structural distortion of the lattice and the formation of a polaron are more pronounced in films with high oxygen deficient and an increased nanocrystallinity (Bange 1999; Zhang et al. 1997). Our TEM images indicate perfect crystallite tungsten oxide nanoparticles in water, hence we apply the small polaron theory to describe absorption in our samples. Peak (2) at $\sim$1.63 eV, shows better in the inset of Fig. 6c for sample $S_{0.5}$, grows by increasing $PdCl_2$ content then decreases and finally disappears. This growth and disappearance take place as the same time as other sharp peaks appear at lower (peak (1)) and higher (peaks (3) and (4)) energies. Two of the peaks are fixed at the position observed in Fig. 6c, peak (1) and peak (3). Fitting the peak (4) with small polaron

theory did lead to very satisfactory results because of its low intensity. The increase in the intensity of fixed peaks continues by increasing the amount of $PdCl_2$. One can assume the enhancement of hydrogen intercalating into the tungsten oxide nanocrystals with increasing $PdCl_2$ content, leading to the intensity growth of polaron absorption peaks. The small polaron absorption mechanism is explained by an optical absorption coefficient as below (Niklasson et al. 2001):

$$\alpha(\mathrm{E}) = (\mathrm{C}/\mathrm{E})exp\left(-\left[\left(\mathrm{E}-2\mathrm{E_p}\right)^2/8\mathrm{E_pE_0}\right]\right) \qquad (2)$$

in which α is the absorption coefficient, C is the constant, E is the photon energy, E_p the polaron energy, and E_0 is the energy related to optical phonons. This equation describes a weakly asymmetric Gaussian peak. A typical fitting curve of $\alpha(E)$ by Eq. 1 for sample S_1 is shown in Fig. 7. This process was applied for all the samples by choosing suitable amounts for C, E_p, and E_0 (Table 1). A slight shift to higher energies can be observed for peak position in Table 1 resulting from the increasing intercalated level because films that undergo increasing intercalation with hydrogen exhibit an absorption peak shift toward higher energies, and similar tendency was reported also for Li and Na (Berggren 2004). This effect may be stronger for peak (2) but due to the appearance of peak (3) there is not clear evidence.

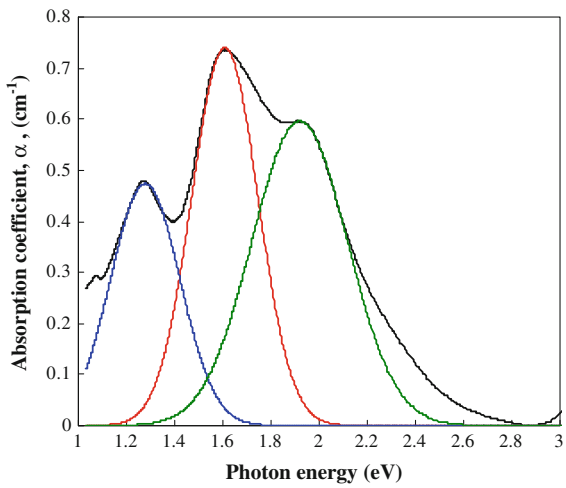

Fig. 7 Curve fitting of different absorption peaks of sample S_1 according to Eq. 2

Coloring kinetics of gasochromic liquid

Time variation curves of optical density (ΔOD) during H_2/O_2 gases exposure for different $PdCl_2$ concentrations are shown in Fig. 8. Since the optical changes of sample $S_{0.5}$ at $\lambda = 632.8$ nm was very low, it was not shown here. For more qualitative analysis the first cycle regions of high and low slopes are shown in Fig. 9. Regions denoted I and II for sample S_1 indicate different coloring velocity; immediately after hydrogen treatment, the rising ΔODs are linear with high slopes almost identical for all samples. After a certain time (depending on $PdCl_2$ content), the slope of curves decreases suddenly and ΔOD seems to approach limits. These limits are not reached during our measurement time, suggesting a late saturation, and thus a great dynamic range of the gasochromic liquid. In region I, a fast process of palladium reduction takes place when hydrogen reaches to the unreacted Pd^{2+} ions of liquid leading to slightly darkening of medium. Region II involves hydrogen interaction with WO_3 nanocrystallites followed by small polaron formation and light absorption which is a slower process.

The particular property of hydrogen is small size of molecule; hence, H_2 has a strong ability of transport in mediums even with almost impermeable properties. Hydrogen molecules rapidly diffuse into the liquid, interacting with Pd ions, generating new Pd particles,

Table 1 Fitting parameters of small polaron absorption according to Eq. 2 for different Pd/WO_3 liquid samples

Sample	E_{max} (eV)	C (eV cm^{-1})	E_p (eV)	E_0 (meV)
$S_{0.5}$	1.63	0.17	0.81	5.5
	1.29	0.61	0.647	7.9
S_1	1.63	1.194	0.81	5.8
	1.93	1.15	0.97	1.0
	1.28	1.26	0.644	11
S_2	1.63	1.52	0.81	10
	1.95	2.05	0.98	6.0
	1.29	1.53	0.65	4.5
S_3	1.68	1.4	0.84	5.5
	1.96	2.3	0.99	8.0
	2.3	0.95	1.15	4.0
	1.3	2.1	0.65	4.5
S_4	1.66	–	–	–
	1.96	3.2	0.99	8.0
	2.3	1.5	1.16	60

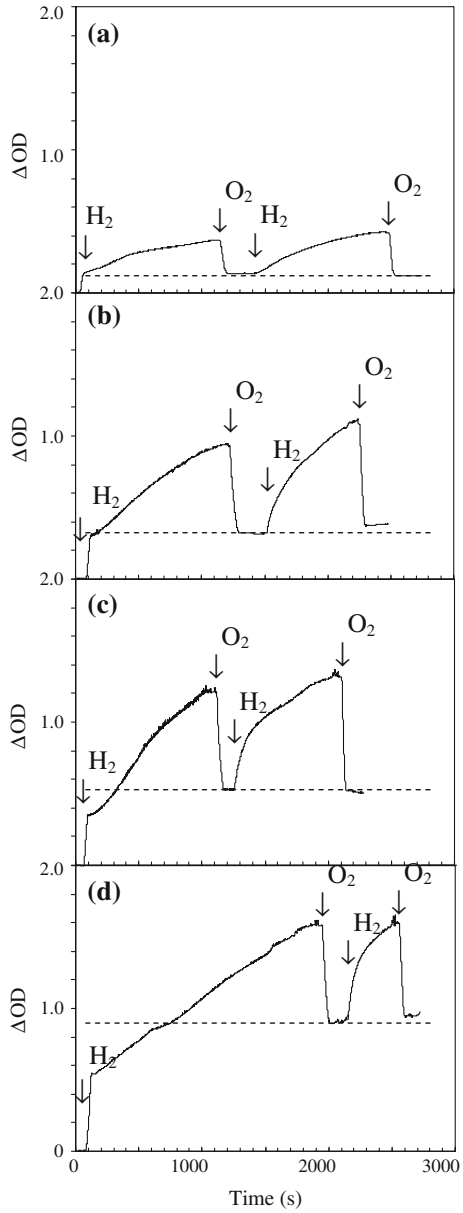

Fig. 8 Time variation of ΔOD at $\lambda = 632.8$ nm for Pd/WO_3 liquid samples with $PdCl_2$ volumes of **a** S_1, **b** S_2, **c** S_3, and **d** S_4

and finally reacting with Pd to produce PdH_x complexes. Even at regular temperature and pressure conditions, the solubility of hydrogen in palladium is high enough to permit the hydrogen absorption up to 900 times of palladium volume. Palladium has lower transmittance than that of its initial $PdCl_2$ before hydrogen reduction, so the fast ΔOD rising at the beginning originates mainly from the Pd producing reactions of those unreacted $PdCl_2$ counterparts in the

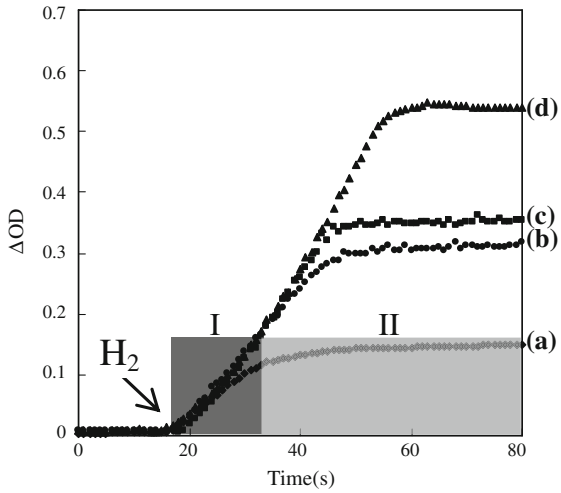

Fig. 9 Time variation near the inset of hydrogen gas for samples **a** S_1, **b** S_2, **c** S_3, and **d** S_4. Regions I and II are identified for sample S_1

liquid or at the tungsten oxide nanocrystals surface as shown in the reaction given below:

$$H_2 + PdCl_2 \rightarrow Pd + 2HCl$$

Rapid gasochromic switching in part I indicate that the above reaction is fast inside the colloidal liquid medium even at room temperature. In part II, slow-rising ΔOD is mainly due to the generation of small polarons in the H_2 intercalated WO_3 nanocrsytals. After certain exposing times of H_2 by which a sufficient coloring was achieved for all samples, pure O_2 was replaced with H_2 gas. By oxygen flushing into the liquid environment, samples start to bleach and the corresponding values of ΔODs decrease to nonzero levels indicating that some colors were left in the liquid. It is expectable because the reduction process of palladium, hence the increased optical absorption of metal Pd is an irreversible process while gasochromic coloring of tungsten oxide nanocrystallites is reversible. The difference between new bleach state and those amounts of ΔOD just at the regions I and II edge increases with the concentration of $PdCl_2$. At the second cycle of coloring, ΔOD start to increase faster compared with that of the first cycle with almost exponential shapes. Furthermore, the coloring rate seems to increase with $PdCl_2$ concentration that is attributed to the catalytic role of Pd against the H_2 molecules. Higher amount of Pd could produce more hydrogen atoms per second near the surface of WO_3 particles. As Fig. 9 shows, the slopes of initial linear

increase are almost the same for all the five samples. Since hydrogen flow was constant at 60 l/h, it seems that a correlation between gas flow and reducing rates may exist. However, the values of ΔOD just at the region I and II edge where the rising slope changes, depend on concentration of $PdCl_2$ which is a result of higher amount of reduced Pd metal in the form of shell or nanoparticles.

Conclusion

In this paper, tungsten oxide nanocrystallites were prepared by laser ablation of tungsten target in DI water, and to produce palladium nanoparticles inside these liquid, $PdCl_2$ solution was added. By XPS analysis, the chemical states of produced nanoparticles were determined to be WO_3. TEM images before adding $PdCl_2$ revealed the presence of WO_3 crystallites with ~40 nm average size. After adding $PdCl_2$, formation of individual Pd or core–shell Pd/WO_3 nanoparticles were observed in which Pd was grown as highly porous shells. An interesting gasochromic effect was observed for Pd/WO_3 samples when hydrogen or oxygen gas was bubbling into the mixed liquid. Optical spectroscopy data of colored samples revealed the formation of different sharp peaks of small polaron absorption below 3 eV in which peak intensities vary with Pd:WO_3 ratio. Production of sharp polaron peaks was attributed to the small size of tungsten oxide nanocrystallites. The dynamic response of coloring was also recorded during alternative bubbling of hydrogen or oxygen gases. Time variation of optical density difference (ΔOD) indicated that at the first coloring cycles extra $PdCl_2$ counterpart reduced to metallic palladium, while the next cycles have an almost normal coloring/bleaching behavior.

References

Abrutis A, Bartasyte A, Garcia G, Teiserskis A, Kubilius V, Saltyte Z, Faucheux V, Figueras A, Rushworth S (2004) Metal-organic chemical vapour deposition of mixed-conducting perovskite oxide layers on monocrystalline and porous ceramic substrate. Thin Solid Films 449(1-2):94–99. doi:10.1016/s0040-6090(03)01404-4

Antonaia A, Polichetti T, Addonizio ML, Aprea S, Minarini C, Rubino A (1999) Structural and optical characterization of amorphous and crystalline evaporated WO_3 layers. Thin Solid Films 354(1–2):73–81

Bange K (1999) Colouration of tungsten oxide films: a model for optically active coatings. Sol Energy Mater Sol Cells 58(1):1–131

Berggren L (2004) Optical absorption and electrical conductivity in lithium intercalated amorphuse tungsten oxide films. Uppsala University, Uppsala

Berhault G, Bausach M, Bisson L, Becerra L, Thomazeau C, Uzio D (2007) Seed-mediated synthesis of Pd nanocrystals: factors influencing a kinetic- or thermodynamic-controlled growth regime. J Phys Chem C 111(16):5915–5925. doi:10.1021/jp0702752

Cantalini C, Sun HT, Faccio M, Pelino M, Santucci S, Lozzi L, Passacantando M (1996) NO_2 sensitivity of WO_3 thin film obtained by high vacuum thermal evaporation. Sens Actuators B 31(1–2):81–87

Colton RJ, Guzman AM, Rabalais JW (1978) Electrochromism in some thin-film transition-metal oxides characterized by X-ray electron spectroscopy. J Appl Phys 49(409):409–416

Di Gregorio F, Keller V (2004) Activation and isomerization of hydrocarbons over WO_3/ZrO_2 catalysts: I. Preparation, characterization, and X-ray photoelectron spectroscopy studies. J Catal 225(1):45–55. doi:10.1016/j.jcat.2004.03.023

Georg A, Graf W, Neumann R, Wittwer V (2000) Mechanism of the gasochromic coloration of porous WO_3 films. Solid State Ion 127(3):319–328. doi:10.1016/s0167-2738(99)00273-8

Granqvist CG (1995) Handbook of inorganic electrochromic materials. Elsevier, Amsterdam

Hu JW, Li JF, Ren B, Wu DY, Sun SG, Tian ZQ (2007) Palladium-coated gold nanoparticles with a controlled shell thickness used as surface-enhanced Raman scattering substrate. J Phys Chem C 111(3):1105–1112. doi:10.1021/jp0652906

Lee SH, Cheong HM, Liu P, Smith D, Tracy CE, Mascarenhas A, Roland Pitts J, Deb SK (2001) Raman spectroscopic studies of gasochromic a-WO_3 thin films. Electrochim Acta 46(13–14):1995–1999. doi:10.1016/s0013-4686(01)00379-6

Li XL, Lou TJ, Sun XM, Li YD (2004) Highly sensitive WO_3 hollow-sphere gas sensors. Inorg Chem 43(17):5442–5449

Martin-Litas I, Vinatier P, Levasseur A, Dupin JC (2002) Characterisation of r.f. sputtered tungsten disulfide and oxysulfide thin films. Thin Solid Films 416(1–2):1–9

Niklasson GA, Granqvist CG (2007) Electrochromics for smart windows: thin films of tungsten oxide and nickel oxide, and devices based on these. J Mater Chem 17(2):127–156. doi:10.1039/b612174h

Niklasson GA, Klasson J, Olsson E (2001) Polaron absorption in tungsten oxide nanoparticle aggregates. Electrochim Acta 46(13–14):1967–1971

Occhiuzzi M, Cordischi D, Gazzoli D, Valigi M, Heydorn PC (2004) WO_x/ZrO_2) catalysts: Part 4. Redox properties as investigated by redox cycles, XPS and EPR. Appl Catal A 269(1–2):169–177. doi:10.1016/j.apcata.2004.04.013

Prasher R, Bhattacharya P, Phelan PE (2005) Thermal conductivity of nanoscale colloidal solutions (nanofluids). Phys Rev Lett 94(2):025901

Ranjbar M, Mahdavi SM, Zad AI (2008a) Pulsed laser deposition of W–V–O composite films: preparation, characterization and gasochromic studies. Sol Energy Mater Sol Cells 92(8):878–883. doi:10.1016/j.solmat.2008.02.018

Ranjbar M, Zad AI, Mahdavi SM (2008b) Gasochromic tungsten oxide thin films for optical hydrogen sensors. J Phys D 41(5). doi:10.1088/0022-3727/41/5/055405

Ranjbar M, Garavand NT, Mahdavi SM, Zad AI (2010) Electroless plating of palladium on WO_3 films for gasochromic applications. Sol Energy Mater Sol Cells 94(2):201–206. doi:10.1016/j.solmat.2009.09.002

Ranjbar M, Fardindoost S, Mahdavi SM, Iraji Zad A, Tahmasebi GN (2011) Palladium nanoparticle deposition onto the WO_3 surface through hydrogen reduction of $PdCl_2$: characterization and gasochromic properties. Sol Energy Mater Sol Cells 95(8):2335–2340. doi:10.1016/j.solmat.2011.04.002

Sakka T, Iwanaga S, Ogata YH, Matsunawa A, Takemoto T (2000) Laser ablation at solid-liquid interfaces: an approach from optical emission spectra. J Chem Phys 112(19):8645–8653

Sasaki T, Shimizu Y, Koshizaki N (2006) Preparation of metal oxide-based nanomaterials using nanosecond pulsed laser ablation in liquids. J Photochem Photobiol A 182(3):335–341. doi:10.1016/j.jphotochem.2006.05.031

Yang GW (2007) Laser ablation in liquids: applications in the synthesis of nanocrystals. Prog Mater Sci 52(4):648–698. doi:10.1016/j.pmatsci.2006.10.016

Zayat M, Reisfeld R, Minti H, Orel B, Svegl F (1998) Gasochromic effect in platinum-doped tungsten trioxide films prepared by the sol–gel method. J Sol Gel Sci Technol 11(2):161–168. doi:10.1023/a:1008645530803

Zhang JG, Benson DK, Tracy CE, Deb SK, Czanderna AW, Bechinger C (1997) Chromic mechanism in amorphous WO_3 films. J Electrochem Soc 144(6):2022–2026